Korea-Australia Rheology Journal
Vol. 18, No. 2, June 2006 pp. 109-118

Deformation characteristics of spherical bubble collapse in Newtonian fluids near the wall using the Finite Element Method with ALE formulation

See Jo Kim, Kyung Hun Lim and Chongyoup Kim[1]*
School of Mechanical Engineering, Andong National University, Andong, Kyungbuk 760-749, Korea
[1]Department of Chemical Biological Engineering, Korea University, Seoul 136-706, Korea
(Received May 18, 2006; final revision received June 5, 2006)

Abstract

A finite-element method was employed to analyze axisymmetric unsteady motion of a deformable bubble near the wall. In the present study a deformable bubble in a Newtonian medium near the wall was considered. In solving the governing equations a structured mesh generator was used to describe the collapse of highly deformed bubbles with the Arbitrary Lagrangian Eulerian (ALE) method being employed in order to capture the transient bubble boundary effectively. In order to check the accuracy of the present FE analysis we compared the results of our FE solutions with the result of the collapse of spherical bubbles in a large body of fluid in which solutions can be obtained using a 1D FE analysis. It has been found that 1D and 2D bubble deformations are in good agreement for spherically symmetric problems confirming the validity of the numerical code. Non-spherically symmetric problems were also solved for the collapse of bubble located near a plane solid wall. We have shown that a microjet develops at the bubble boundary away from the wall as already observed experimentally. We have discussed the effect of Reynolds number and distance of the bubble center from the wall on the transient collapse pattern of bubble.

Keywords : ALE method, cavitation, microjet, wall effect

1. Introduction

The deformation of bubbles in Newtonian or non-Newtonian fluids has been of great importance in many engineering problems. It has been also of theoretical interests. The deformation of vapor bubbles has been the subject of many theoretical and experimental researches due to its close relationship with cavitation phenomena and subsequent deformation and collapse in the shear flow field. Especially the shock wave and microjet generated during the fast collapse of bubble are responsible for the cavitation damage of impellers of ships and pumps (Plesset and Prosperetti, 1977; Hammitt, 1980; Blake and Gibson, 1987). It has been reported many years ago that cavitation is substantially reduced and the cavitation damage is also reduced in drag reducing polymer solutions (Ellis *et al.*, 1970). Slight viscoelasticity of the dilute polymer solution appears to reduce both the cavitation phenomenon and cavitation damage because both the time scale of the bubble collapse and the material time of the polymer solution have the orders of a millisecond, hence the Deborah number has an order of 1.

Until now only a few theoretical and numerical analyses on viscoelastic fluids have been reported for the collapse of cavitation bubbles (Yoo and Han, 1982; Kim, 1994), even when spherical symmetry is maintained. Many problems regarding bubble collapse near the wall still remain open questions. Moreover, the numerical analysis for bubble collapse near the wall is not easy especially in the viscoelastic fluids. For bubbles in viscoelastic fluids the partial differential equations themselves are always nonlinear, and therefore the boundary integral method is not easy to be applicable. It might be worth noting that most of recent results were obtained using boundary integral methods (Plesset and Chapman, 1971; Blake and Gibson, 1987; Blake *et al.*, 1993). In this regard, the present study by using the finite method has paved a way for simulating the bubble collapse in the viscoelastic fluids, which will be the next subject in our research.

In the present study a deformable bubble in a Newtonian medium near the wall is considered. To the best of our knowledge, no work has previously been reported on the computation of flow of a bubble in Newtonian liquid in an axisymmetric flow near the wall using the FEM together with the Arbitrary Lagrangian Eulerian (ALE) method. Very recently we have developed FEM computer codes for this problem, specifically, using FEM together with an unstructured mesh generation with the auto-remeshing technique (Kim, 2000; Kim and Han, 2001; Kim *et al.*,

*Corresponding author: cykim@grtrkr.korea.ac.kr

2003). In the present study the FE method using the structured mesh with the ALE method is introduced in order to capture the transient bubble boundary effectively together with the SU/PG scheme for stabilizing the convection terms. In order to check the proper implementation of the present FE code we compare the results of our FE solutions with the results of the collapse of spherical bubbles in the large body of fluid in which solutions can be obtained using a 1D FE analysis. In this paper we have discussed the effect of the Reynolds number and geometric distance of the bubble from the wall on the transient collapse pattern.

2. Governing equations and boundary conditions

The most general situation describing dispersed liquid-bubble two-phase flow, can be represented by the continuity and momentum equations:

$$\nabla\cdot\mathbf{v}_m = 0\ ;\ \rho_m\left(\frac{\partial\mathbf{v}_m}{\partial t}+\mathbf{v}_m\cdot\nabla\mathbf{v}_m\right) = -\nabla\cdot\delta p_m+\nabla\cdot\boldsymbol{\sigma}_m \tag{1}$$

$$\nabla\cdot\mathbf{v}_b = 0\ ;\ \rho_b\left(\frac{\partial\mathbf{v}_b}{\partial t}+\mathbf{v}_b\cdot\nabla\mathbf{v}_b\right) = -\nabla\cdot\delta p_b+\nabla\cdot\boldsymbol{\sigma}_b \tag{2}$$

in which ∇ is the gradient operator, δ is the Kronecker delta operator, $\mathbf{v}$ is velocity vector, ρ is the density of fluid, p is pressure, $\boldsymbol{\sigma}$ is extra stress tensor, and subscripts m and b on the variables denote the matrix phase and dispersed phase (*i.e.*, bubble), respectively. In the case of very fast diffusion, the pressure inside the gas may be assumed constant during the entire bubble collapse. We have assumed that the suspending medium is incompressible and the bubble has the very fast diffusion process. Then we do not have to solve the equations inside the bubble.

Equation (1) can be rewritten in dimensionless form by dropping the subscript m for the medium as

$$\nabla^*\cdot\mathbf{v}^* = 0 \tag{3}$$

$$\mathrm{Re}\left(\frac{\partial\mathbf{v}^*}{\partial t^*}+\mathbf{v}^*\cdot\nabla\mathbf{v}^*\right) = -\nabla^*\cdot\delta p^*+\nabla^*\cdot\boldsymbol{\sigma}^* \tag{4}$$

in which the dimensionless variables (with asterisks) are defined by

$$\nabla^* = R_i\nabla;\ \mathbf{v}^* = \mathbf{v}/V_0;\ t^* = t/t_0;\ p^* = p/(\bar{\eta}V_0/R_i);$$
$$\boldsymbol{\sigma}^* = \boldsymbol{\sigma}/(\bar{\eta}V_0/R_i) \tag{5}$$

with R_i (initial bubble radius), V_0, and $t_0 = R_i/V_0$ being the characteristic length, velocity, and time, and $\bar{\eta}$ being the viscosity of fluids. In Eq. (4), $\mathrm{Re} = \rho_m V_0 R_i/\bar{\eta}$ is the Reynolds number.

We begin with the simple problem of axisymmetric flow of a bubble of radius R_i in a large body of incompressible Newtonian fluid, as schematically shown in Fig. 1. In this problem, there are three boundaries, the first one (S_1) consisting of the imaginary outer boundary where a constant pressure, p_0, is applied, and the second one (S_2) being the portion of the interface between the bubble and the suspending medium where surface tension plays an important role, and the other one (S_3) being the rigid wall. However, on S_2, neither the velocity nor the traction is known *a priori*. Therefore, at this interface, appropriate relationships must be specified in terms of the interfacial conditions for the shear stress and normal balances. At the interface between the bubble and the liquid, the following normal stress and shear stress balances, respectively, must be satisfied:

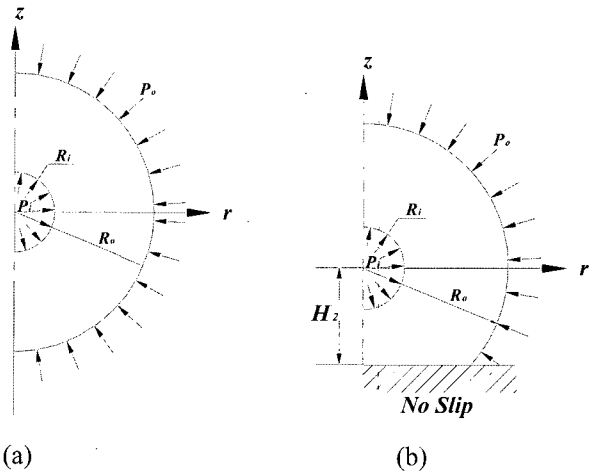

Fig. 1. Schematic diagram describing two types of the geometry and boundary condition: (a) without wall, (b) with wall.

$$\text{(i)}\ t_i n_j \sigma_{ij}^* = 0 \tag{6}$$

$$\text{(ii)}\ (-p^*\delta+\boldsymbol{\sigma}^*)\cdot\mathbf{n}-(-p_i^*\delta)\cdot\mathbf{n} = \frac{\mathrm{H}^*}{\mathrm{Ca}}\mathbf{n} \tag{7}$$

where $\mathbf{t}$ and $\mathbf{n}$, respectively, are the local unit tangential and outward normal vectors to the interface, $\mathrm{H}^* = R_i/R$ with R being the local radius of curvature, and $\mathrm{Ca} = \bar{\eta}V_0R_i/\gamma$ is the capillary number, and γ being the interfacial tension.

The pressure at the imaginary outer boundary is constant: $\mathrm{P}_0 = 1$, and the position of the outer boundary far from the initial bubble radius, say 15 times R_i being chosen as 1, *i.e.*, $\mathrm{R}_i = 1$, $\mathrm{R}_0 = 15$, and the initial condition at $t = 0$ is $\mathbf{v}_m = 0$, and no-slip boundaries are applied at the wall as shown in Fig. 1.

3. Formulation of finite element equations

Detailed description of the computational algorithm for the two-phase moving problem can be found in papers (Kim, 2000; Kim and Han, 2001; Kim *et al.*, 2003), which used the FEM together with an unstructured mesh generator with the auto-remeshing technique. In this paper we use the structured mesh with the ALE scheme. That is, in

dealing with a moving boundary problem such as bubble deformation during collapse, an effective numerical algorithm(s) is essential for obtaining reliable numerical results. In carrying out numerical computations we have to develop numerical algorithms to calculate the shape (*i.e.*, interfacial positions) of bubble, and generate the structured finer meshes as the extent of bubble deformation increases near the wall, especially when the Re number is high. In addition, the convective term, $v\cdot\nabla v$, can be treated using the ALE formulation to simulate the moving bubble boundary in this simulation of the bubble collapse. The convective term, $v\cdot\nabla v$, in the momentum equation in Eq. (4) can be implemented to simulate the moving bubble boundary via the ALE description during the bubble collapse as $(v-v^m)\cdot\nabla v$ where v^m indicates the mesh velocity. With doing this and by introducing the shape function ϕ for velocities and ψ for pressure, respectively, one can easily obtain the following expression by using the Galerkin finite element method in the ALE description for the continuity and momentum equation, respectively, as follows:

$$\int_{V_1^*} v_{i,i}^* \psi dV^* = 0 \tag{8}$$

$$\int_{V^*} \mathrm{Re}\frac{\partial v_i^*}{\partial t^*}\phi dV^* + \int_{V^*} \mathrm{Re}(v_j^* - v_j^{m^*})\frac{\partial v_i^*}{\partial x_j^*}\phi dV^* + \int_{V^*} \phi_{,j}(-p^*\delta_{ij} + v_{j,i} + v_{i,j})dV^* - \int_{S_1^*} \tau_i^*\phi dS^* - \int_{S_2^*} \tau_i^*\phi dS^* = 0 \tag{9}$$

where ϕ is the quadratic shape function for velocity and ψ is the linear shape function for pressure, respectively, and x_j represents r and z, respectively, for $j=1$ and 2, in the cylindrical coordinate system. The last term on the right-hand side of Eq. (9) includes the inner pressure and the interfacial tension as given in Eq. (7). The second term involving the convection on the left-hand side of Eq. (9) indicating the ALE formulation was numerically obtained using the streamline upwinding/Petrov Galerkin (SU/PG) method as the stabilization scheme.

In Eq. (7) and (9) the term containing Ca and the dimensionless curvature H^* does not depend on the velocity and can thus be considered as a forcing vector in the FEM formulation. After employing a standard assembly procedure, from Eq. (8) and (9) one can obtain the global finite element matrix equations that can be solved for the velocity and pressure fields.

To obtain finite-element matrix equations, nine-node isoparametric rectangular elements were employed with a quadratic shape function for the velocity and the velocity gradient and four-node linear shape functions for the pressure as follows:

$$v_r^* = \phi(\zeta,\eta)_j v_{rj}^*, \quad v_z^* = \phi(\zeta,\eta)_j v_{zj}^*, \quad j=1-9 \tag{10a}$$

$$p^* = \psi(\zeta,\eta)_j p_j^*, \quad j=1,2,3,4. \tag{10b}$$

Velocity components expressed in terms of local coordinates (t, n) defined along the surfaces S_1^* must be transformed into the global coordinates (r, z) in order to apply the pressure in the normal direction of the imaginary outer boundary expressed in terms of local coordinates (t, n) as,

$$\{V\} = [Q]\{\bar{V}\} \tag{11}$$

where [Q] is a coordinate transformation matrix, {V} is a vector of the variables in the global coordinates, and $\{\bar{V}\}$ is a vector of the variables in the local coordinates (Kim and Kwon, 1995).

At each time step, a modified Newton-Raphson method (Kim and Kwon, 1995) was used to obtain the numerical solution and the following convergence criterion was used

$$\sum_{i=1}^{n} |u_i^{r+1} - u_i^r|^2 / \sum_{i=1}^{n} |u_i^{r+1}|^2 < 10^{-8} \tag{12}$$

where n is the total number of nodes and r appearing in the superscript denotes the r-th iteration. In the present study, the convergence criterion was satisfied with $r \approx 15$.

4. Numerical results and discussion

In the derivation of equations in Sec. 3, the interfacial tension term has been included for completeness. However, it will be set to be zero in the numerical calculation in this section for simplicity. The problem solved here is that of an initially spherical bubble near the solid wall. Using the discretized equations and numerical algorithms presented above, we have computed the deformed shape of bubble during collapse.

Before comparing the computed bubble shapes near the wall we will first compare the results of our finite element solutions without the wall as depicted in Fig. 1(a) with the results of 1D FEM simulation in the paper of Kim (1994), who considered the collapse of a spherical cavitation bubble in a large body of the Newtonian and upper convected Maxwell fluid using 1D FEM. With doing this we will discuss the accuracy of the finite element method developed in this study.

Fig. 2(a) shows the initial structured mesh and Fig. 2(b) and (c) represent the middle and final meshes during the ALE computation. To check the accuracy of the numerical solution, collapse patterns in Newtonian fluids are examined first for several different meshes. We omitted the discussion on convergence depending on different meshes in this paper since there were no computational problems during simulation as we expected. In Fig. 3, evolutions for bubble collapse of FEM solution obtained in this research are shown for several different Re values together with 1D FEM results in order to compare them. It is seen that no bubble oscillation takes place in the Newtonian fluid while the oscillatory pattern of bubble collapse takes place only in a viscoelastic fluid as discussed in the paper (Yoo and

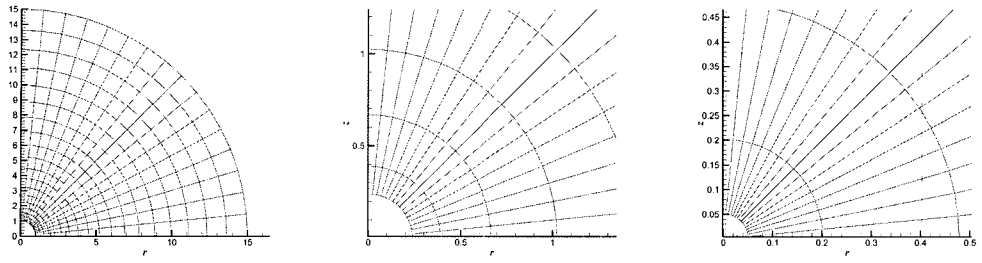

(a) (b) (c)

Fig. 2. Initial (a), middle (b) and final (c) stages of mesh shapes in using ALE method.

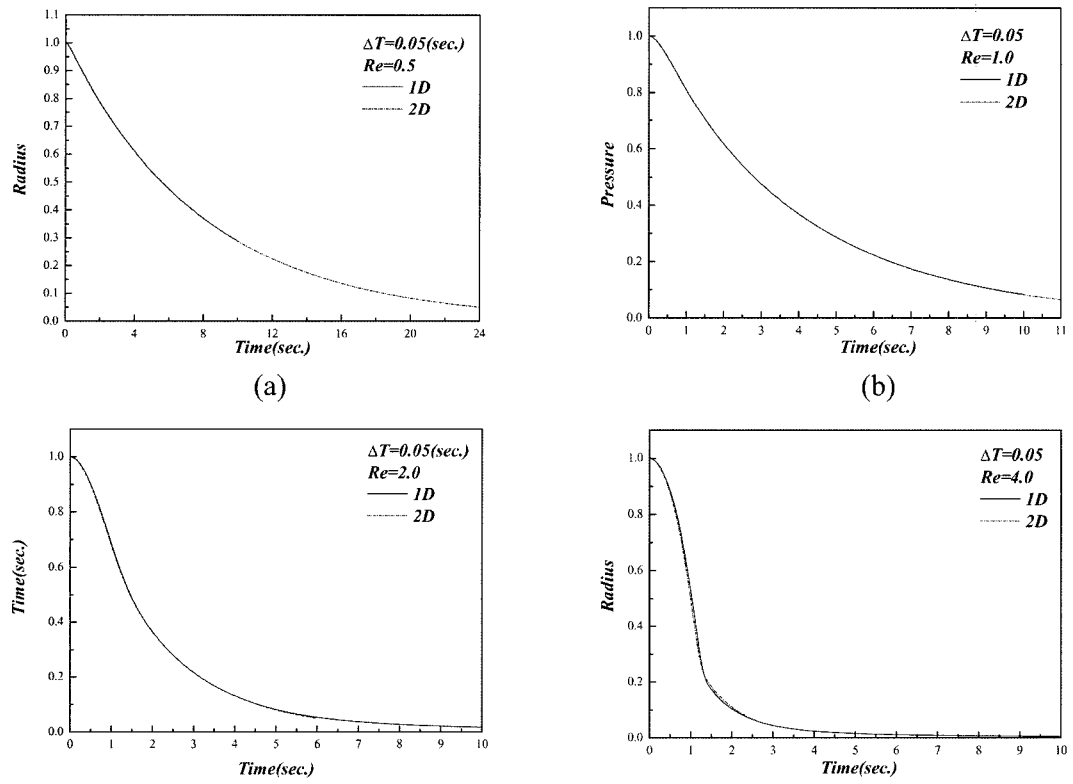

Fig. 3. Bubble collapse in a Newtonian fluid for several Re numbers.

Han, 1982; Kim, 1994). As the Re number increases the speed of bubble collapse dramatically increases. In Fig. 4, the evolutions of bubble pressure on the bubble interface in the medium are shown for several different Re values together with 1D FEM results. As the Re number increases collapse proceeds faster and the peak in pressure increases and this value converges to a constant value which is the same as the pressure at the imaginary outer boundary. From results in Figs. 3-4, one can see that results obtained by the current ALE formulation and ones by 1-D Lagrangian formulation in Kim (1994) are in good agreement, and hence it can be concluded the FEM code developed here gives quite an accurate solutions.

There have been several previous numerical investigations of the bubble collapse problem near a wall. Most notable studies among earlier works were carried out by Plesset and Chapman (1971) and Mitchell and Hammit (1973), who obtained the bubble deformation during collapse near the wall without considering the fluid viscosity. Fig. 5(a) shows the initial structured mesh and Fig. 5(b) represents the final stage of mesh patterns after the ALE computation. It was found that a stable numerical solution could not be obtained at each time step as the bubble collapses especially for the higher Re number if not provided with an optimal grid density around the bubble interface. As shown in Fig. 5(a) the initial grid distribution is rel-

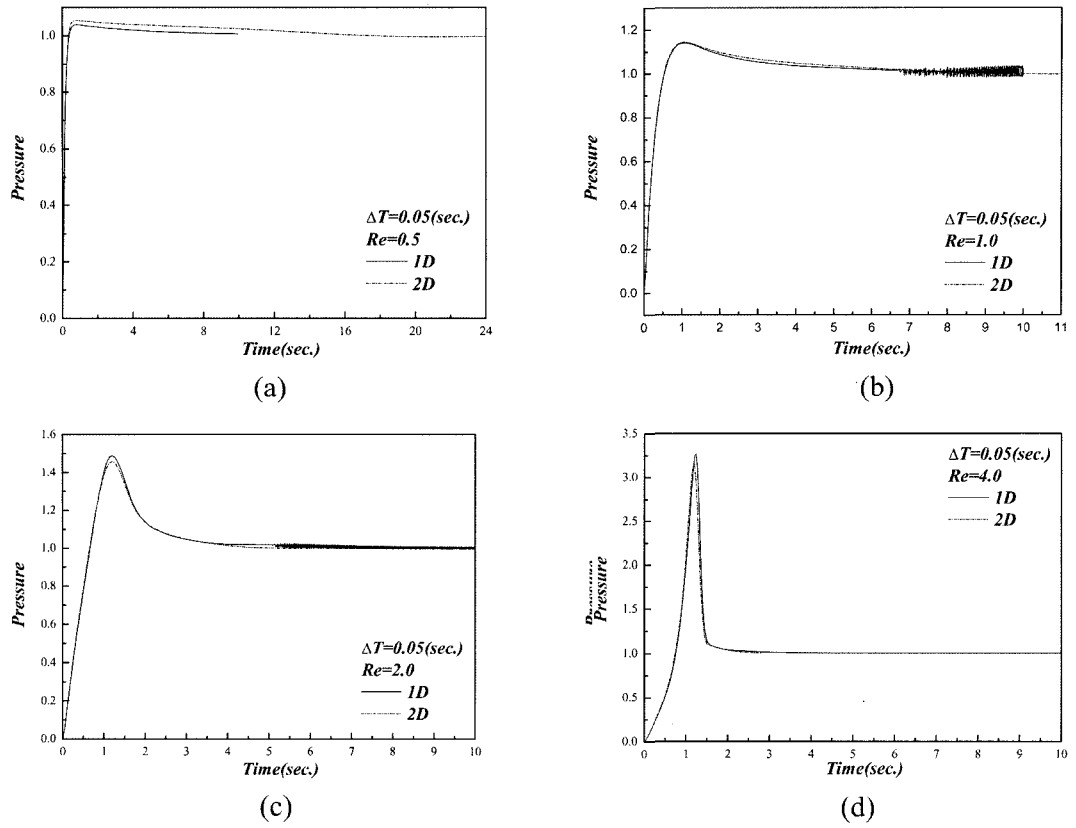

Fig. 4. The medium fluid pressure on the interface during bubble collapse in a Newtonian fluid for several Re numbers.

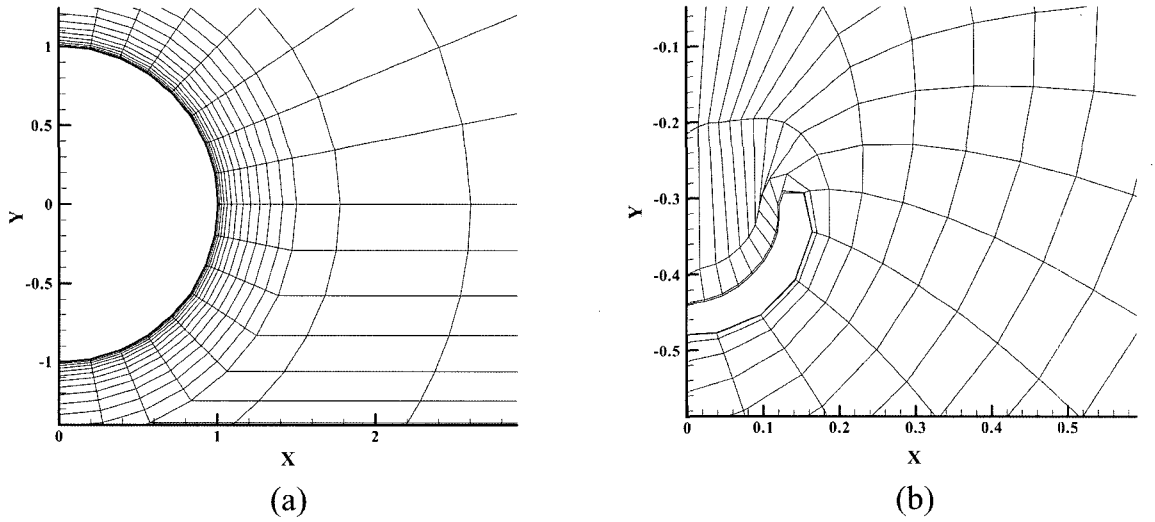

Fig. 5. Initial (a) and final (b) stage mesh shape to simulate the bubble collapse near the wall at Re = 200 with $H_2 = 1.5$.

atively simple to obtain the reasonable numerical result. During the bubble collapse this kind of grid pattern should be kept to obtain a finer solution as shown in Fig. 5(b).

The collapse of an initially spherical bubble near the wall was simulated for several different Re numbers and different geometries, that is, the different locations from the wall, H_2 as depicted in Fig. 1 and Fig. 7 show the velocity field and pressure contours, respectively, obtained at the final stage of bubble collapse, *i.e.*, just before the liquid jet penetrates the opposite side of the bubble, near the wall at Re = 200 for two different H_2: (a) $H_2 = 1.3$, (b) $H_2 = 1.1$. Fig. 6 shows that the maximum magnitude of the velocity

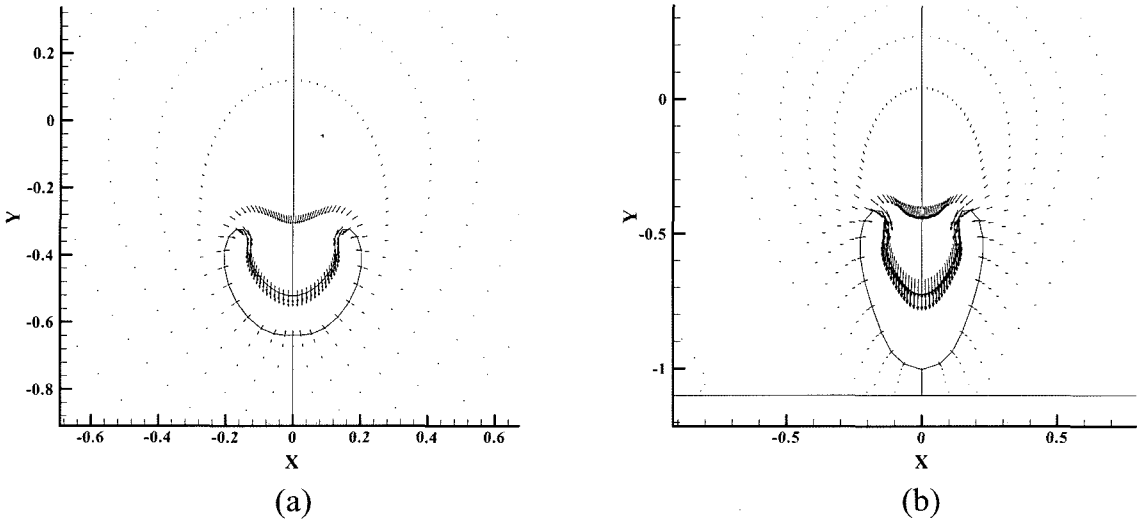

Fig. 6. Velocity field at the final stage of bubble collapse near the wall at Re = 200 for two different H_2: (a) $H_2 = 1.3$, (b) $H_2 = 1.1$.

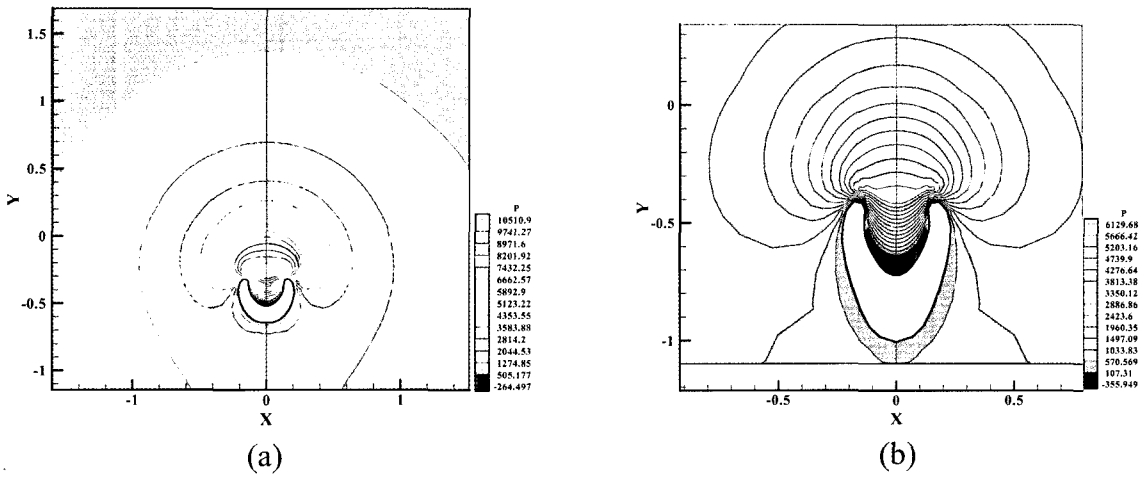

Fig. 7. Pressure contours at the final stage of bubble collapse near the wall at Re = 200 for two different H_2: (a) $H_2 = 1.3$, (b) $H_2 = 1.1$.

field is at the tip of the liquid jet as expected. Fig. 7 shows that the point of maximum pressure is located above the liquid jet. It is seen that the stand-off distance affects the pressure distribution on the rigid wall, which is more dominant as the value of H_2 decreases. The pressure contour and velocity field distribution for high Re number, say, 200, are well matched with the results by Plesset and Chapman (1971) and Mitchell and Hammit (1973) for inviscid flows.

Fig. 8 shows the evolution of bubble boundary at several time steps during the collapse near the rigid wall for four different stand-off distances with the dimensionless time step, $\Delta t^* = 0.001$ at Re = 200: (a) $H_2 = 2.0$, (b) $H_2 = 1.5$, (c) $H_2 = 1.3$, (d) $H_2 = 1.1$. In Fig. 8, the dimensionless time increment among the computed shapes of a bubble is 0.1 except the final stage of the bubble. The dimensionless time at the final stage of the bubble is 0.964 for $H_2 = 2.0$, 0.997, for $H_2 = 1.5$, 1.014 for $H_2 = 1.3$, and 1.0385 for $H_2 = 1.1$, respectively. The stand-off distance, H_2 influences the bubble deformation during the collapse as shown in Fig. 8. The bottom of the bubble still moves upwards towards the bubble center for $H_2 = 2.0$, $H_2 = 1.5$, $H_2 = 1.3$. However, when H_2 reduces to 1.1, the centroid of the bubble moves towards the wall dramatically displaying the well-known Bjerknes effect while the bottom of the bubble remains unmoved. Deformation patterns of the bubble near the wall during collapse for high Re number, say, 200 in this study, are well matched with the results by Plesset and Chapman (1971) and Mitchell and Hammit (1973) for inviscid flows. In this case of high Re value one can imagine that the formation of jet should be the result of the asymmetric deformation caused by the presence of the wall

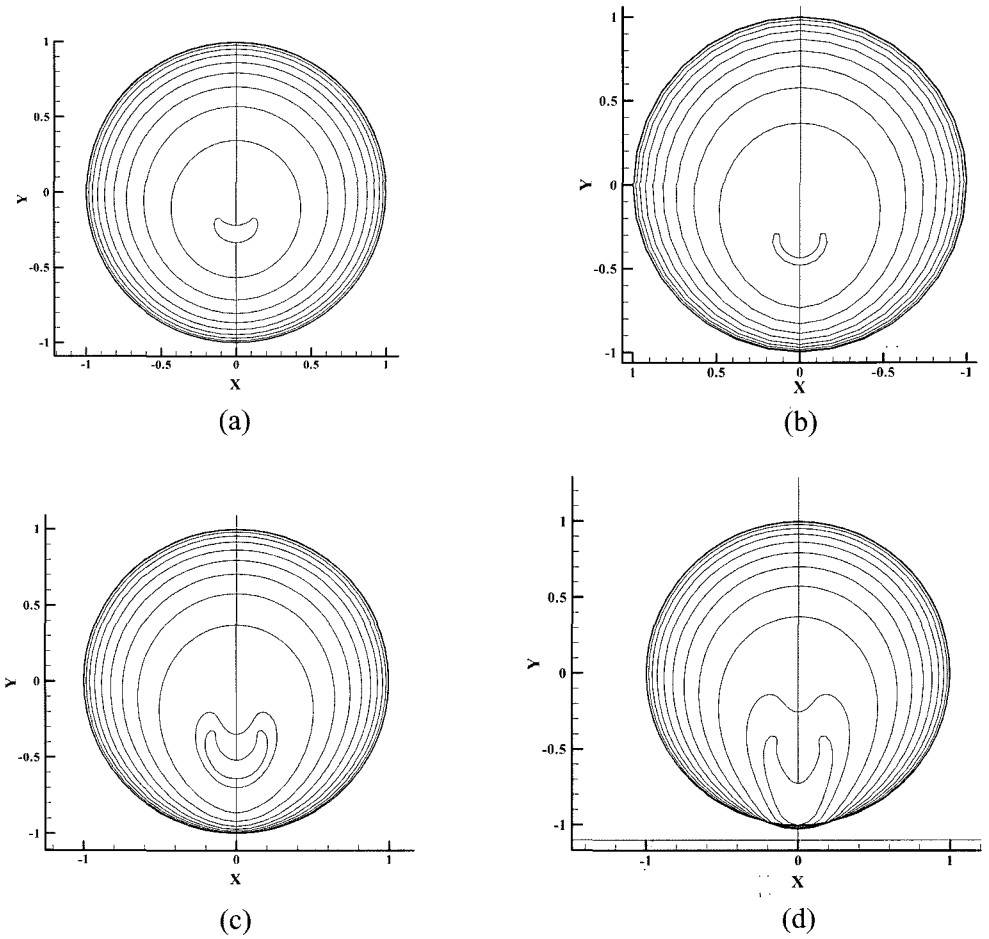

Fig. 8. Evolution of collapse for the bubble profile at several times during the collapse near the rigid wall for four different stand-off distances with the dimensionless time step, $\Delta t^* = 0.001$ at Re = 200: (a) $H_2 = 2.0$, (b) $H_2 = 1.5$, (c) $H_2 = 1.3$, (d) $H_2 = 1.1$.

during the collapse. To examine the deformation of a bubble more closely, some enlarged bubble shapes near the final stage of collapse are also shown in Fig. 9. Other system parameters are the same as in Fig. 8. When the rigid wall is located relatively far from the bubble as in Fig. 9(a), the bubble collapses less asymmetrically while yielding a higher speed liquid jet directed towards the wall. However, the stand-off distance increases, the impact strength of liquid jet will be reduced.

The results on the bubble collapse near the wall in this numerical study are accurate when compared with the numerical models based on the motion of an incompressible inviscid liquid (Plesset and Chapman, 1971; Mitchell and Hammit, 1973). The stand-off distance, H_2, controls the bubble sphericity: the farther the bubble is from the wall, the more spherical it remains at least initially. However, the jet velocity increases as the bubble is located farther from the wall.

In order to see the Re number effect on the jet formation at low Re regime, Fig. 10 illustrates the evolution of the bubble profile at several time steps during the collapse near the rigid wall for four different Re numbers with the dimensionless time step, $\Delta t^* = 0.01$ and the time increment of 2: (a) Re = 0.5, (b) Re = 1.0, (c) Re = 2.0, (d) Re = 4.0. Comparing Fig. 10 with Fig. 9 one can recognize the influence of the Re number on jet formulation. For a high Re number the jet velocity is high to hit the other side of the bubble boundary. On the other hand, for a low Re number, the initial velocity is small and the bubble interface never impacts the other side of bubble as shown in Fig. 10. There is a strong elongation of the bubble in the direction of the centerline of the bubble and takes a long time for collapse. Therefore, from our numerical results in Fig. 10, one can confirm that the viscous effect is dominant for moderate to low Re numbers (below order of one).

At high Re number, the liquid jet at the final stage of the collapse of a cavitation bubble hits the rigid wall if it is originally attached to the wall or penetrates the lower boundary of the bubble if it is located away from the wall as shown in Fig. 8 and 9, resulting in a doughnut-shaped bubble (Brujan *et al.*, 2002). In this situation one cannot continue the computation any further, which reflects the

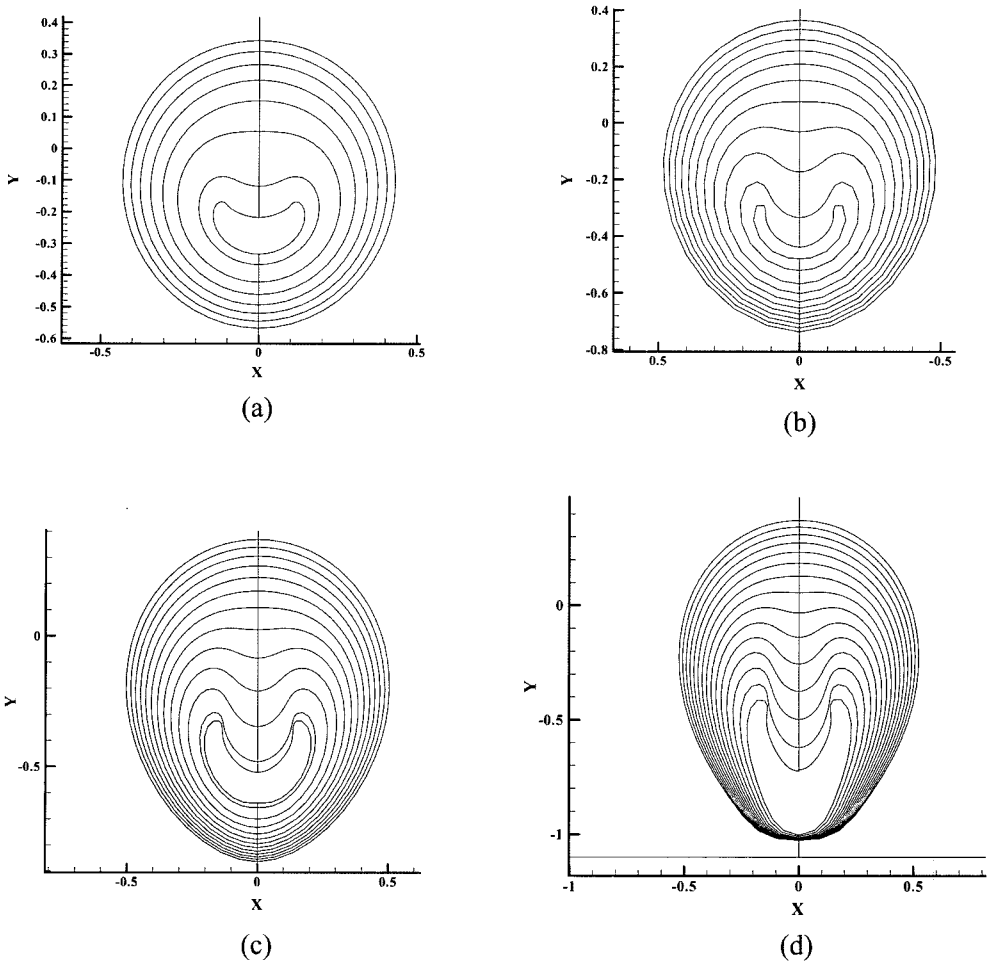

Fig. 9. Enlarged bubble shapes near the final stage of collapse: (a) from $t^* = 0.90$ to 0.96 with time increment of 0.01 and $t^* = 0.964$ at the final stage of collapse, (b) from $t^* = 0.90$ to 0.99 with time increment of 0.01 and $t^* = 0.997$ at the final stage of collapse, (c) from $t^* = 0.90$ to 1.01 with time increment of 0.01 and $t^* = 1.014$ at the final stage of collapse, (d) from $t^* = 0.90$ to 1.00 with time increment of 0.01 and $t^* = 1.0385$ at the final stage of collapse. Other system parameters are the same as in Fig. 8.

limitation of the front tracking algorithm used in the current study. In order to remedy this problem, one needs to introduce the interface capturing algorithm in a purely Eulerian framework instead of the front tracking method in ALE framework, such as the volume-of fluid (VOF) method, the level-set method, and the diffuse-interface method. In the next study, we will present the liquid jet penetration problem mentioned above using the level-set method developed in the ongoing study (Kim and Hwang, 2006) algorithm in a purely Eulerian framework.

5. Concluding remarks

Since analytical methods are not amenable to solve such complex problems for bubble collapse, one must resort to numerical methods such as finite element analysis. We have presented an original numerical technique to solve accurately the Navier-Stokes equation with free-surfaces using the finite element method with ALE methods. In the present study we successfully computed large-deformation of a bubble collapse, suspended in the Newtonian liquid by first formulating finite element matrix equations and then developing efficient ALE algorithms implemented for the moving interface of the collapse bubble with a two-dimensional structured mesh generator. In formulating finite element equations we used the Galerkin method with SU/PG for treating the convection term in the ALE description. At each time step the ALE method was used to track the interface of bubble. We have demonstrated the accuracy of the finite-element system equations formulated in this study by comparing the results of our finite element solutions with the 1D FEM simulations by Kim (1994) for spherically symmetric cases without wall effects.

In this paper we have discussed the effects of Re number, especially at high (200) and low (0.5-4) values on the computed shapes of deformed bubbles collapsing axisymmet-

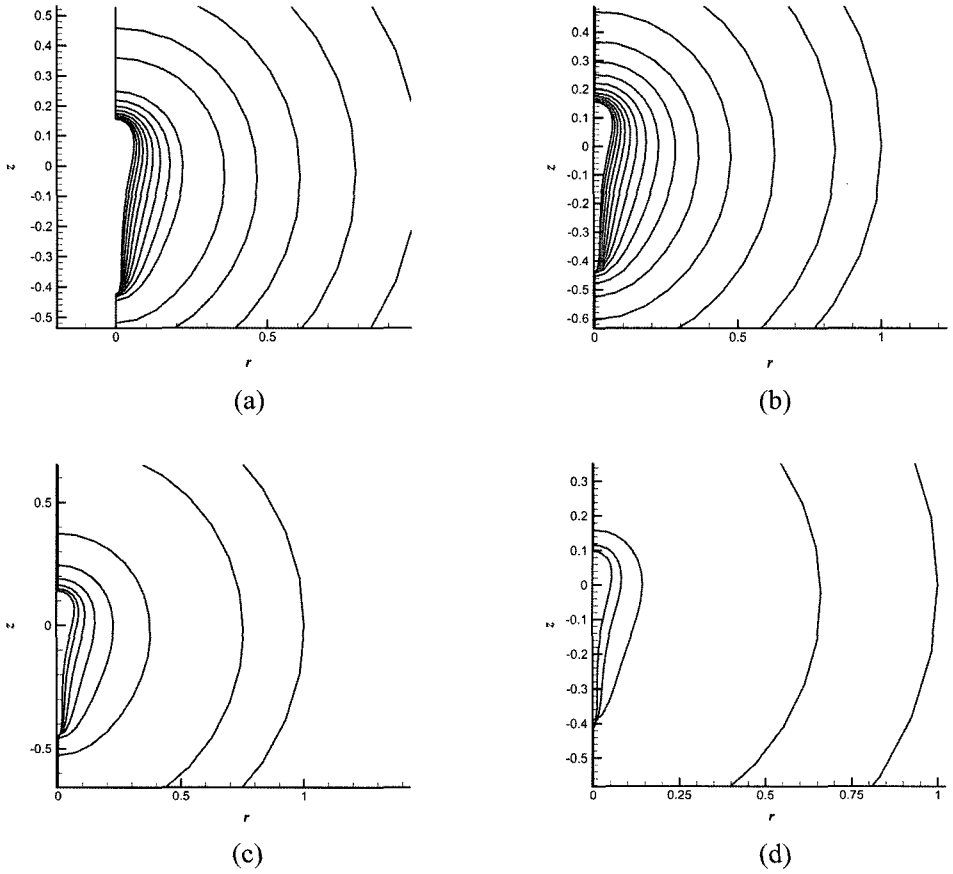

Fig. 10. Evolution of collapse for the bubble profile at several times during the collapse near the rigid wall for four different Re numbers with the dimensionless time step, $\Delta t^* = 0.01$ and the time increment of 2: (a) Re = 0.5, (b) Re = 1.0, (c) Re = 2.0, (d) Re = 4.0.

rically near a plane solid wall. In addition, detailed numerical studies of the effect of the stand-off distance value, H_2 on the deformation of the bubble during collapse have been discussed.

The majority of viscoelastic bubbles exhibits the oscillation mode due to the elastic properties of liquid. Therefore, future studies must include the effect of fluid elasticity on bubble deformation. In this regard, we believe that the present study has paved a way for attacking the bubble dynamics in the viscoelastic fluid, which is the highly challengeable research topic in this area.

Acknowledgment

This study was supported by the 2004 special program of Andong National University.

References

Blake, J.R. and D.C. Gibson, 1987, Cavitation bubbles near boundaries, *Annu. Rev. Fluid Mech.* **19**, 99-123.

Blake, J.R., P.B. Robinson, A. Shima and Y. Tomita, 1993, Interaction of two cavitation bubbles with rigid boundary, *J. Fluid Mech.* **255**, 707-721.

Brujan, E.A., G.S. Keen, A. Vogel and J.R. Blake, 2002, The final stage of the collapse of a cavitation bubble close to a rigid boundary, *Phys. Fluids* **14**, 85-92.

Ellis, A.T., J.G. Waugh and R.Y. Ting, 1970, Cavitation suppression and stress effects in high speed flows of water with dilute macromolecule additives, *Trans. ASME, J. Basic Eng.* **92**, 459.

Hammit, F.G., 1980, Cavitation and Multiphase Flow Phenomena, McGraw-Hill, New York.

Kim, C., 1994, Collapse of spherical bubbles in Maxwell fluids, *J. Non-Newtonian Fluid Mech.* **55**, 37-58.

Kim, S.J and W.R. Hwang, 2006, Direct numerical simulation of drop emulsions in sliding bi-periodic frames using the level set method, *J. Comp. Phys.* in preparation.

Kim, S.J., 2000, Development of a finite element method with auto-remeshing techniques for analysis of the droplet deformation in a two-phase polymeric mixture, *J. Korean Fiber Soc.* **37**, 234-241.

Kim, S.J. and C.D. Han, 2001, Finite element analysis of axisymmetric creeping motion of a deformable non-Newtonian drop in the entrance region of a cylindrical tube, *J. Rheol.* **45**, 1279-1303.

Kim, S.J., S.D. Kim and Y. Kwon, 2003, Deformation non-New-

tonian drops in the entrance region, *Korea-Australia Rheol. J.* **15**, 75-82.

Kim, S.J. and T.H. Kwon, 1995, Development of numerical simulation methods and analysis of extrusion processes of particle-filled plastic materials subject to slip at the wall, *Powder Technol.* **85**, 227-239.

Mitchell, T.M. and F.H. Hammit, 1973, Asymmetric cavitation bubble collapse, *Trans. ASME J. Fluids Eng.* **95**, 29-37.

Plesset, M.S. and A. Prosperetti, 1977, Bubble dynamics and cavitation, *Annu. Rev. Fluid Mech.* **9**, 145-185.

Plesset, M.S. and R.B. Chapman, 1971, Collapse of an initially spherical vapour cavity in the neighbourhood of a solid boundary, *J. Fluid Mech.* **47**, 283-290.

Yoo, H.J. and C.D. Han, 1982, Oscillatory behavior of a gas bubble growing (or collapsing) in viscoelastic liquids, *AIChE J.* **28**, 1002-1009.